Spectrochimica Acta Part A 82 (2011) 191–199

Contents lists available at ScienceDirect

Spectrochimica Acta Part A: Molecular and Biomolecular Spectroscopy

journal homepage: www.elsevier.com/locate/saa

Synthesis, spectroscopic, antimicrobial, DNA binding and cleavage studies of some metal complexes involving symmetrical bidentate N, N donor Schiff base ligand

D. Arish, M. Sivasankaran Nair*

Department of Chemistry, Manonmaniam Sundaranar University, Tirunelveli 627 012, India

ARTICLE INFO

Article history:
Received 12 February 2011
Received in revised form 4 June 2011
Accepted 7 July 2011

Keywords:
Schiff base
IR
CV
Antimicrobial activity
DNA

ABSTRACT

The Schiff base ligand, *N*,*N*′-bis-(4-isopropylbenzaldimine)-1,2-diaminoethane (L), obtained by the condensation of 4-isopropylbenzaldehyde and 1,2-diaminoethane, has been used to synthesize the complexes of the type $[ML_2X_2]$ [M = Co(II), Ni(II) and Zn(II); X = Cl and OAc]. The newly synthesized ligand (L) and its complexes have been characterized on the basis of elemental analyses, mass, ^{1}H and ^{13}C-NMR, molar conductance, IR, UV–vis, magnetic moment, CV and thermal analyses, powder XRD and SEM. IR spectral data show that the ligand is coordinated to the metal ions in a bidentate manner. The geometrical structures of these complexes are found to be octahedral. Interestingly, reaction with Cu(II) ion with this ligand undergoes hydrolytic cleavage to form ethylenediamine copper(II) complex and the corresponding aldehyde. The antimicrobial results indicate that the chloro complexes exhibit more activity than the acetato complexes. The complexes bind to CT–DNA by intercalation modes. Novel chloroform soluble ZnL_2Cl_2 complex exhibits tremendous antimicrobial, DNA binding and cleaving properties.

1. Introduction

The chelating structures, moderate electron donation and easy tunable electronic and steric effects proved Schiff bases as versatile ligands capable of stabilizing different metals in various oxidation states with unusual structural features [1–7]. The chemistry of Schiff base ligands and their metal complexes have attracted a lot of interest due to their facile synthesis and wide range of applications including antifungal, antibacterial, anticancer and catalytic fields [8–11]. The interaction of transition metal compounds with DNA has been extensively studied due to the unusual binding, cleaving properties and general photoactivity [12,13]. These coordination compounds have been found to be suitable candidates as DNA secondary structure probes, photocleavers and antitumor drugs [14,15]. Further, for the development of metallo drug as chemotherapeutic agents, it is essential to explore the interactions of metal complexes with DNA [16]. In this paper, we report the synthesis, characterization and biological studies of Co(II), Ni(II) and Zn(II) complexes with *N*,*N*′-bis-(4-isopropylbenzaldimine)-1,2-diaminoethane Schiff base ligand.

2. Experimental

2.1. Materials

4-isopropylbenzaldehyde was obtained from Himedia. 1,2-diaminoethane was purchased from Merck and used without further purification. Calf Thymus (CT) and pUC19 DNA was obtained from Genei, Bangalore. Co(II), Ni(II), Cu(II) and Zn(II) chlorides/acetates were Merck samples. All other reagents and solvents were purchased from commercial sources and were of analytical grade.

2.2. Synthesis of Schiff base ligand

To a solution of 4-isopropylbenzaldehyde (2 mmol) in methanol (20 ml), 1,2-diaminoethane (1 mmol) in methanol (20 ml) was added dropwise. The above mixture was magnetically stirred for about 6 h and the resulting yellow colour solution was kept in a beaker. After one day, yellow colored crystals were separated out. It was washed with cold alcohol, ether and recrystallized from ethanol. Yellow solid; Yield: 92%. Anal. Calcd. for $C_{22}H_{28}N_2$: C 82.45, H 8.81, N 8.74; found C 82.56, H 8.72, N 8.72; GC–MS (*m*/*z*): 321.2 $[M+H^+]$; ^{1}H-NMR ($CDCl_3$, ppm): $-CH_3$ (12H, d, δ 1.288), –CH– (2H, m, δ 2.956), $-CH_2-$ (4H, s, 3.941), –CH– (aromatic) (4H, d, δ 7.249; 4H, d, δ 7.605), –CH=N– (2H, s, δ 8.512); ^{13}C-NMR ($CDCl_3$, ppm): $-CH_3$ (4C, δ 23.746), –CH– (2C, δ 34.022), –CH– (aromatic) (12C, δ

* Corresponding author. Tel.: +91 9443540046; fax: +91 462 23334363.
E-mail address: msnairchem@rediffmail.com (M.S. Nair).

1386-1425/$ – see front matter © 2011 Elsevier B.V. All rights reserved.
doi:10.1016/j.saa.2011.07.031

110-154), –CH=N– (2C, δ 162.427); IR (υ, cm^{-1}): –C=N– (1648); UV–vis (λ_{max}, nm): 236, 295.

2.3. Synthesis of the Schiff base metal(II) complexes

Schiff base ligand (2 mmol) was dissolved in methanol (20 ml) and metal(II) chloride/acetates (1 mmol) in methanol (20 ml) was added dropwise with constant stirring. The above mixture was magnetically stirred for about 6–8 h. The solid product formed was filtered off, washed several times with ether and cooled in vacuum desiccator over fused anhydrous calcium chloride.

$[CoL_2Cl_2]$: violet solid; yield: 78%: anal. calcd. for $C_{44}H_{56}N_4Cl_2Co$: C 68.56, H 7.32, N 7.27, Cu 7.65; found C 68.33, H 7.52, N 7.58, Co 7.08; m.p: >250 °C; DART–MS (*m*/*z*):770.6542 $[M^+]$; IR (υ, cm^{-1}): –C=N– (1638), M–N (452); UV–vis (λ_{max}, nm): 590, 659; Λc (Ω^{-1} cm^2 mol^{-1}): 12; μ_{eff} (B.M): 4.91.

$[CoL_2(OAc)_2]$: violet solid; yield: 81%: anal. calcd. for $C_{48}H_{62}N_4O_4Co$: C 70.48, H 7.64, N 6.85, Cu 7.20; found C 70.41, H 7.69, N 6.67, Co 7.27; m.p: >250 °C; DART–MS (*m*/*z*): 817.9197 $[M^+]$; IR (υ, cm^{-1}): –C=N– (1640), COO^- (1610, 1402), M–N (449), M–O (510); UV–vis (λ_{max}, nm): 592, 650; Λc (Ω^{-1} cm^2 mol^{-1}): 8.0; μ_{eff} (B.M): 5.13.

$[NiL_2Cl_2]$: green solid; yield: 64%: anal. calcd. for $C_{44}H_{56}N_4Cl_2Ni$: C 68.73, H 7.24, N 7.27, Ni 7.65; found C 68.33, H 7.52, N 7.58, Ni 7.57; m.p: >250 °C; DART–MS (*m*/*z*):770.5743 $[M^+]$; IR (υ, cm^{-1}): –C=N– (1640), M–N (438); UV–vis (λ_{max}, nm): 378, 710, 1100; Λc (Ω^{-1} cm^2 mol^{-1}): 4.0; μ_{eff} (B.M): 2.87.

$[NiL_2(OAc)_2]$: light green solid; yield: 80%: anal. calcd. for $C_{48}H_{62}N_4O_4Ni$: C 70.50, H 7.64, N 6.85, Ni 7.18; found C 70.71, H 7.61, N 6.64, Ni 7.32; m.p: >250 °C; DART–MS (*m*/*z*): 817.6523 $[M^+]$; IR (υ, cm^{-1}): –C=N– (1640) COO^- (1604, 1392), M–N (451), M–O (530); UV–vis (λ_{max}, nm): 390, 728, 1100; Λc (Ω^{-1} cm^2 mol^{-1}): 7.0; μ_{eff} (B.M): 2.93.

$[ZnL_2Cl_2]$: white solid; yield: 92%. anal. calcd. for $C_{44}H_{56}N_4Cl_2Zn$: C 67.99, H 7.26, N 7.21, Zn 8.41; found C 67.93, H 7.64, N 7.28, Ni 7.98; m.p: >250 °C; DART–MS (*m*/*z*): 777.3645 $[M^+]$; ^{1}H-NMR ($CDCl_3$, ppm): –CH_3 (12H, d, δ 1.279), –CH– (2H, m, δ 2.974), –CH_2– (4H, s, 4.029), –CH– (aromatic) (4H, d, δ 7.418; 4H, d, δ 7.944), –CH=N– (2H, s, δ 8.675); ^{13}C-NMR ($CDCl_3$, ppm): –CH_3 (4C, δ 23.590), –CH– (2C, δ 34.436), –CH_2– (2C, δ 59.815), –CH– (aromatic) (12C, δ 126–156), –CH=N– (2C, δ 169.468); IR (υ, cm^{-1}): –C=N– (1642), M–N (461); UV–vis (λ_{max}, nm):237, 290; Λc (Ω^{-1} cm^2 mol^{-1}): 12.0.

$[ZnL_2(OAc)_2]$: white solid; yield: 92%: anal. calcd. for $C_{48}H_{62}N_4O_4Zn$: C 69.93, H 7.58, N 6.80, Ni 7.93; found C 70.11, H 7.70, N 6.64, Ni 8.12; m.p: >250 °C; DART–MS (*m*/*z*): 824.6312 $[M^+]$; ^{1}H-NMR ($CDCl_3$, ppm): –CH_3 (12H, d, δ 1.278), –CH– (2H, m, δ 2.971), –CH_2– (4H, s, 4.039), –CH– (aromatic) (4H, d, δ 7.412; 4H, d, δ 7.938), –CH=N– (2H, s, δ 8.677); ^{13}C-NMR ($CDCl_3$, ppm): –CH_3 (4C, δ 23.590), –CH– (2C, δ 34.436), –CH_2– (2C, δ 59.815), –CH– (aromatic) (12C, δ 126–156), –CH=N– (2C, δ169.732); IR (υ, cm^{-1}): –C=N– (1640) COO^- (1612, 1418), M–N (437), M–O (517); UV–vis (λ_{max}, nm):236, 289; Λc (Ω^{-1} cm^2 mol^{-1}): 9.0.

2.4. Physical measurements

Elemental analyses were done using a Perkin-Elmer elemental analyzer. The GC mass spectrum of the Schiff base ligand was recorded on a GC–MS/MS Varian Saturn 2200 GC-Varian CP 3800 spectrometer. The DART–MS was recorded on a JEOL-AccuTOF JMS-T100LC mass spectrometer having a DART (Direct Analysis in Real Time) source. The metal contents in the complexes were determined by standard EDTA titration [17]. Molar conductance of the complexes were measured in MeOH (10^{-3} M) solutions using a coronation digital conductivity meter. IR spectra were recorded in KBr discs on a JASCO FT/IR-410 spectrometer in the 4000–400 cm^{-1} region. The electronic spectra were recorded on a Perkin Elmer Lambda-25 UV–vis spectrometer. Room temperature magnetic measurements were performed on a Guoy's balance by making diamagnetic corrections using Pascal's constant. Cyclic voltammetric measurements were carried out in a Bio-Analytical System (BAS) model CV-50W electrochemical analyzer. The three-electrode cell comprised of a reference Ag/AgCl, auxiliary platinum and working glassy electrodes. Tetrabutylammonium perchlorate was used as supporting electrolyte. Thermal analysis was carried out on a Perkin-Elmer thermal analyzer with a heating rate of 20 °C/min using N_2 atmosphere. Powder XRD was recorded on a Rigaku Dmax X-ray diffractometer with Cu-Kα radiation ($\lambda_{K\alpha}$ = 1.5406 Å). SEM images were recorded in a Hitachi SEM analyzer.

2.5. Antimicrobial activities

Antibacterial and antifungal activities of the ligand and its complexes were tested *in vitro* against the bacterial species *Escherichia coli, Bacillus subtilis, Pseudomonas aeruginosa* and *Staphylococcus aureus*; fungal species, *Aspergillus niger, Aspergillus flavus* and *Candida albicans* by the disc diffusion method [18]. All the species used were of ATCC. The test organisms were grown on nutrient agar for anti bacterial and potato dextrose agar medium for antifungal in petri plates. The compounds were prepared in DMF and soaked in filter paper disc of 5 mm diameter and 1 mm thickness. The discs were placed on the previously seeded plates and incubated at 37 °C and the diameter of inhibition zone around each disc was measured after 24 h for antibacterial and 72 h for antifungal activities. The standard error for the experiment is ±0.001 cm and the experiment is repeated three times under similar conditions. DMF is used as negative control and *Amikacin, Ofloxacin* and *Ciprofloxacin* were used as positive standards for antibacterial and *Nystatin* for antifungal activities. The minimum inhibitory concentration (MIC) was determined by serial dilution technique.

2.6. DNA binding experiments

A solution of CT–DNA in 0.5 mM NaCl/5 mM Tris-HCl (pH 7.0) gave a ratio of UV absorbance at 260 and 280 nm (A260/A280) of 1.8–1.9, indicating that the DNA was sufficiently free of proteins. A concentrated stock solution of DNA was prepared in 5 mM Tris-HCl/50 mM NaCl in water at pH 7.0 and the concentration of CT–DNA was determined per nucleotide by taking the absorption coefficient (6600 dm^3 mol^{-1} cm^{-1}) at 260 nm [19]. Stock solutions were stored at 4 °C and were used only for a maximum of 4 days. Doubly distilled water was used to prepare buffer solutions. Solutions were prepared by mixing the complex and CT–DNA in DMF medium. Absorption titrations were performed by keeping the concentration of the complex constant (10 μM) and by varying the concentration of CT–DNA from 0 to 25 μM. The binding constant (K_b) for the complexes have been determined from the following equation [19]

$$\frac{[DNA]}{(\varepsilon_A - \varepsilon_F)} = \frac{[DNA]}{(\varepsilon_B - \varepsilon_F)} + \frac{1}{K_b(\varepsilon_B - \varepsilon_F)}$$

where ε_A, ε_B and ε_F correspond respectively to the apparent, bound and free metal complex extinction coefficients. A plot of $[DNA]/(\varepsilon_A - \varepsilon_F)$ versus [DNA] gave a slope of $1/(\varepsilon_B - \varepsilon_F)$ and a *Y*-intercept equal to $1/K_b(\varepsilon_B - \varepsilon_F)$, where K_b is the ratio of slope to the intercept.

2.7. Gel electrophoresis

The pUC19 DNA (1 μg), 10 μM metal complex, 50 μM H_2O_2 in 50 mM Tris-HCl buffer (pH 7.1) were mixed. The contents

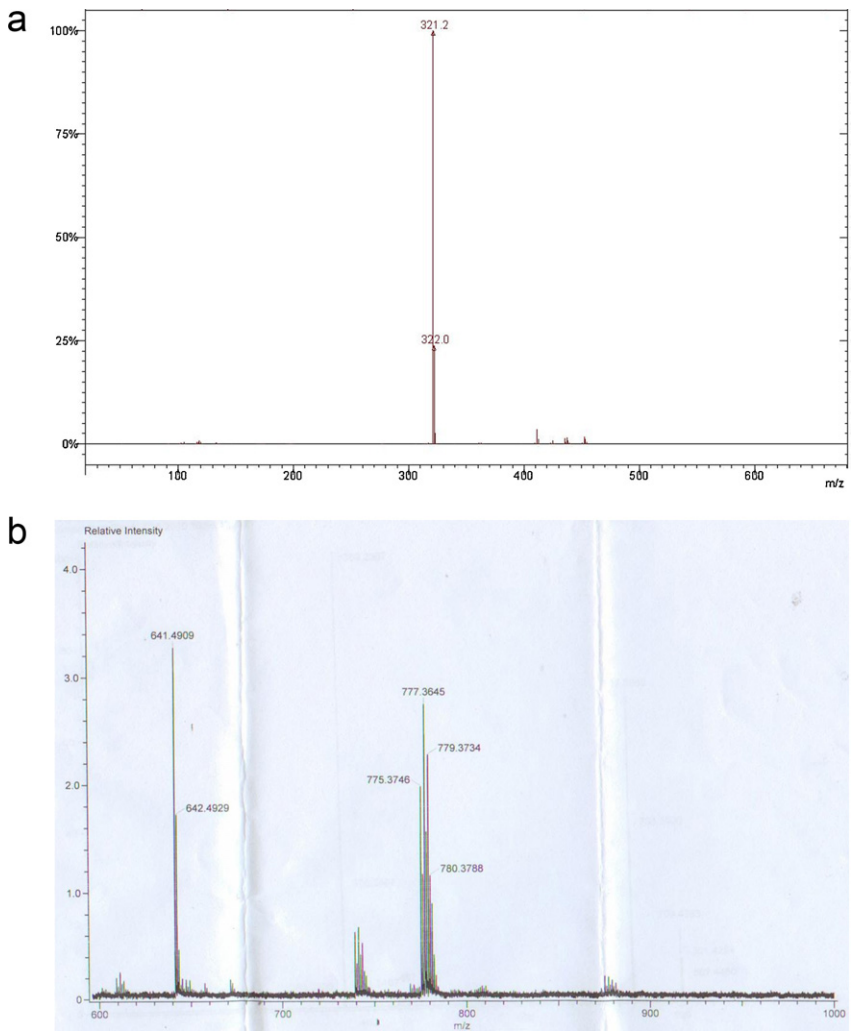

Fig. 1. (a) GC-Mass spectrum of the Schiff base ligand (L). (b) DART-Mass spectrum of $[ZnL_2Cl_2]$ complex.

were incubated for 30 min at 37 °C and loaded on 0.8% Agarose gel after mixing 5 μl of loading buffer (0.25% bromophenol blue + 0.25% Xylene cyanol + 30% glycerol sterilized distilled water). Electrophoresis was performed at constant voltage (100 V) until the bromophenol blue reached to one third of the gel. The gel was stained for 10 min by immersing in an ethidium bromide solution. The gel was then detained for 10 min by keeping in sterilized distilled water and the plasmid bands visualized by photographing the gel under a UV transilluminator. The efficiency of DNA cleavage was measured by determining the ability of the complex to form open circular (OC) or nicked circular (NC) DNA from its super coiled (SC) form.

3. Results and discussion

The analytical data and physical properties of the ligand and its complexes are given in experimental Sections 2.2 and 2.3. The elemental analyses data confirm the assigned composition of the ligand and its complexes. The Schiff base is soluble in all common organic solvents except water. All the complexes are stable at room temperature, insoluble in water, but soluble in MeOH, DMF, DMSO and MeCN. The Zn(II) complexes are highly soluble in chloroform. The low molar conductivity values of the metal complexes are given in experimental Section 2.3 suggests their non-electrolytic nature [20].

3.1. Mass spectra

The GC–MS of Schiff base (Fig. 1a) shows a well-defined molecular ion peak at 321.2 ($M+H^+$), which coincides with formula weight of the Schiff base. The DART mass spectrum of CoL_2Cl_2, NiL_2Cl_2, ZnL_2Cl_2, $CoL_2(OAc)_2$, $NiL_2(OAc)_2$ and $ZnL_2(OAc)_2$ complexes shows a peak at *m/z* 770.6542(4%), 770.5743(2.1%), 777.3645(2.8%), 817.9197(4%), 817.6523(4%) and 824.6312(2.2%), respectively, corresponding to their molecular weights. The mass spectrum of all the complexes indicates that the complexes are monomeric confirming the metal to ligand ratio to be 1:2 in the complexes. The representative mass spectrum of ZnL_2Cl_2 complexes is shown in Fig. 1b.

3.2. NMR spectra

The NMR spectral data of the ligand and its Zn(II) complexes are given in experimental Sections 2.2 and 2.3. The ^1H and ^{13}C-NMR spectrum of the ligand and its ZnL_2Cl_2 is shown in Figs. 2a and b and 3a and b. As shown in Fig. 2a, it is observed that the signal for azomethine proton (>CH=N–) in the ligand appears as a singlet at 8.512 ppm. The peaks at 1.288 and 2.596 ppm are assignable to the isopropyl –CH– and $–CH_3$ protons, respectively. The aromatic ring protons are observed in the 7–8 ppm range as expected. The ^{13}C-NMR spectrum of Schiff base ligand shows a peak at 162.427 ppm characteristic of azomethine carbon. In the ^1H and

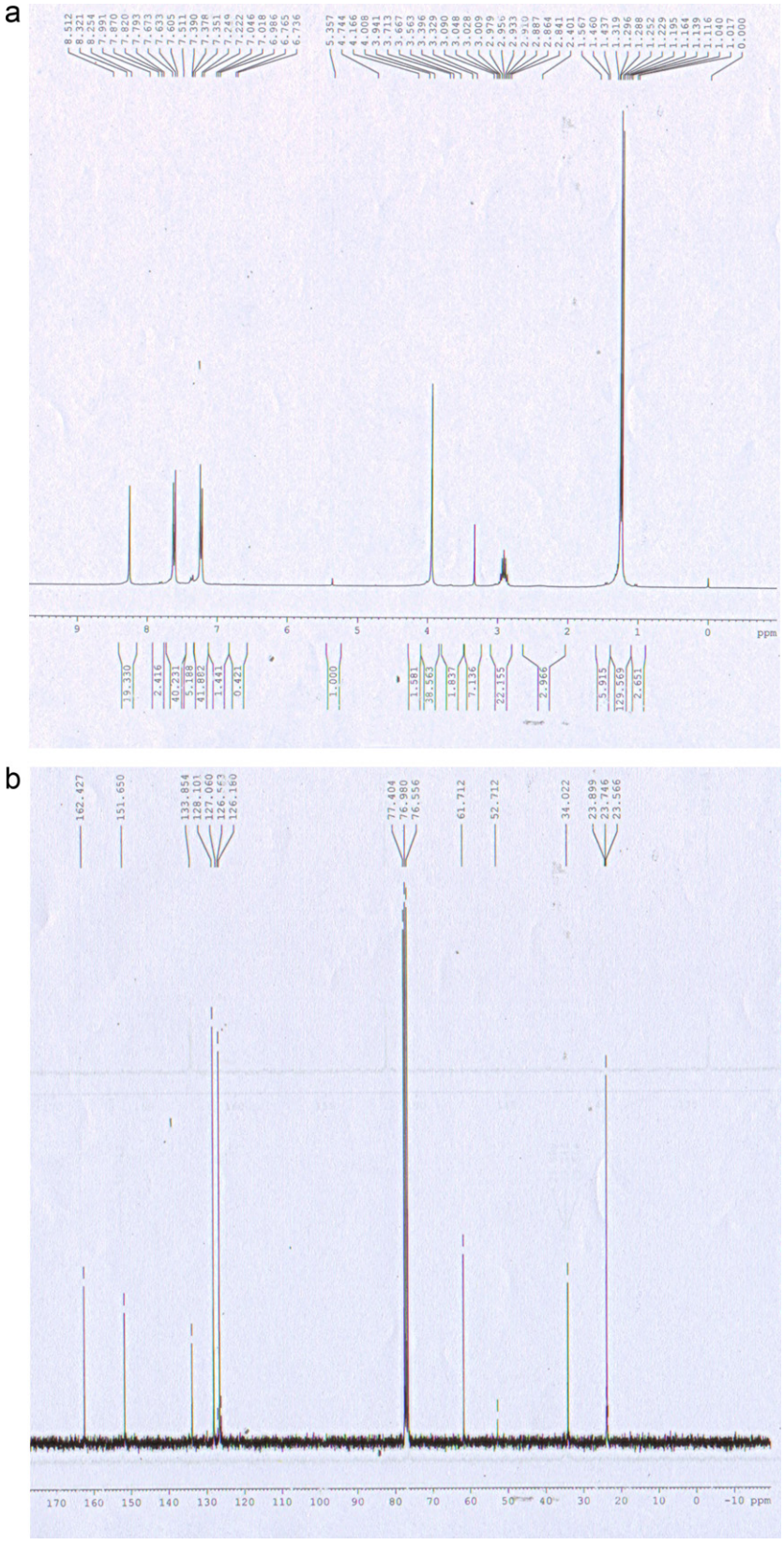

Fig. 2. (a) ^{1}H-NMR spectrum of the Schiff base ligand (L). (b) ^{13}C-NMR spectrum of the Schiff base ligand (L).

^{13}C-NMR spectrum of Zn(II) complexes, the azomethine (–CH=N–) proton and carbon peaks are shifted to downfield which indicates the metal to coordinate the ligand through azomethine nitrogen atom.

3.3. IR spectra

The IR spectrum of the free ligand exhibits a sharp band at 1648 cm^{-1}, due to the azomethine group vibration. On com-

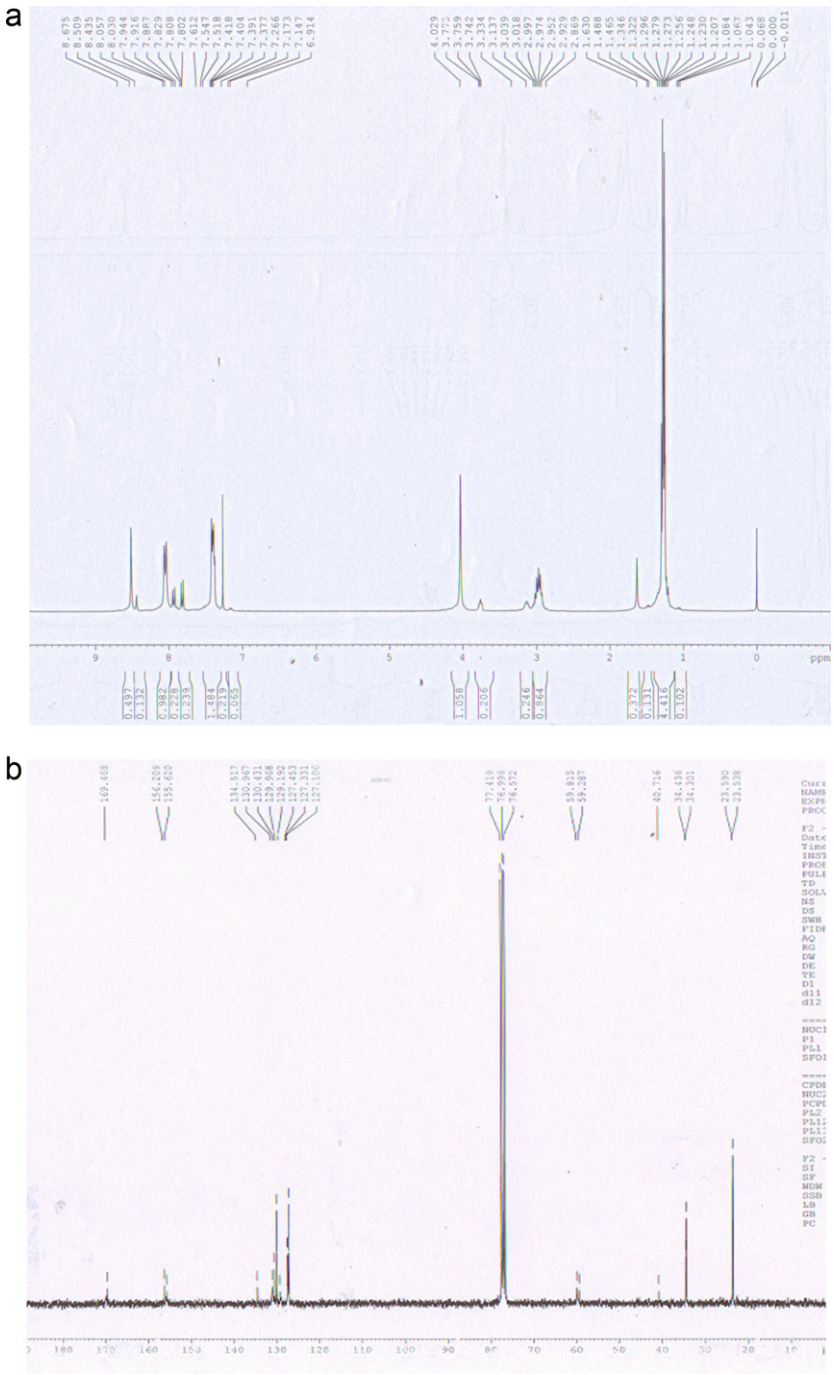

Fig. 3. (a) ^{1}H-NMR spectrum of $[ZnL_2Cl_2]$ complex. (b) ^{13}C-NMR spectrum of $[ZnL_2Cl_2]$ complex.

plexation this band was shifted to lower frequency in the ~1642–1638 cm^{-1} range indicating the coordination of the azomethine nitrogen atom to the metal ion. In addition several strong sharp bands at 2990–2940 cm^{-1} range can be ascribed to υ(C–H) vibration of the isopropyl group. In the acetato complexes, the bands at 1612–1605 and 1418–1392 cm^{-1} can be attributed to the asymmetric and symmetric stretching vibration of the acetate group. The large difference between the $\upsilon_{as}(CH_3COO^-)$ and $\upsilon_s(CH_3COO^-)$ value of ~200 cm^{-1} indicates the monodentate binding nature of the acetato group [21,22]. The weak bands observed at 461–430 cm^{-1} can be assigned to the ν(M–N) vibration [22].

3.4. Electronic spectra and magnetic measurements

In the electronic spectrum of the ligand, the broad band centered at 295 nm is assigned to π–π^* transition of the azomethine (>C=N) chromophore. In addition, the other intense absorption broad band centered at 236 nm is due to the π–π^* and n–π^* transition of the benzene ring of the Schiff base ligand. The electronic spectrum of Co(II) complexes show two absorption bands at 550–700 nm region (experimental Section 2), which are assignable to $^4T_{1g}(F) \rightarrow {}^4A_{2g}(F)$ and $^4T_{1g}(F) \rightarrow {}^4T_{2g}(F)$ transitions in an octahedral environment [23]. The magnetic susceptibility value is found to be 4.91 and 5.13 B.M for CoL_2Cl_2 and $CoL_2(OAc)_2$, respectively.

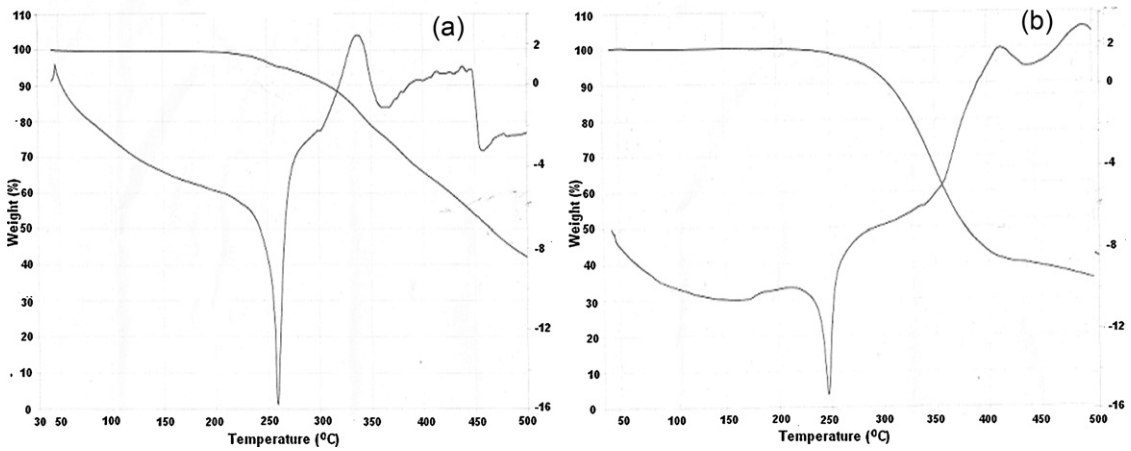

Fig. 4. TG–DTA curves of (a) $[CoL_2Cl_2]$; (b) $[CoL_2(OAc)_2]$ complexes.

This is comparable with that of 4.3–5.2 B.M expected for octahedral Co(II) complexes, indicative of octahedral geometry for the present Co(II) complexes [24]. The electronic spectrum of the Ni(II) complexes show three bands in the region ~1100, ~700 and ~400 nm, attributable to $^3A_{2g}(F) \rightarrow {}^3T_{2g}(F)$, $^3A_{2g}(F) \rightarrow {}^3T_{1g}(F)$ and $^3A_{2g}(F) \rightarrow {}^3T_{1g}(P)$ transitions, respectively, suggesting an octahedral geometry around Ni(II) atom [24]. The NiL_2Cl_2 and $NiL_2(OAc)_2$ complexes reported herein are found to have a room temperature magnetic moment value of 2.87 and 2.93 B.M respectively, which are in the range of 2.9–3.3 B.M observed for octahedral Ni(II) complexes [24].

3.5. Electrochemistry

The cyclic voltammograms were recorded in acetonitrile solution at a scan rate of 100 mV s^{-1} in the potential range +2.0 to −2.0 V. The cyclic voltammogram of CoL_2Cl_2 shows a well defined redox process corresponding to the formation of the quasi-reversible Co(II)/Co(I) couple. The cathodic peak at −689 mV versus Ag/AgCl and the associated anodic peak at −240 mV correspond to the Co(II)/Co(I) couple. The peak-to-peak separation (ΔE_p = 449 mV) indicates quasi-reversible one electron transfer process. The redox property of $CoL_2(OAc)_2$ displayed electrochemically reversible Co(II)/Co(I) reduction peak at −703 mV and the associated oxidation peak at −258 mV corresponds to the Co(II)/Co(I) quasi-reversible process. The peak-to-peak separation (ΔE_p) is 445 mV indicating the process to be quasi-reversible. The electrochemistry of NiL_2Cl_2 is similar to that of $NiL_2(OAc)_2$, anodic waves are seen at −810 and at −838 mV and the associated cathodic peaks at −692 and −678 mV respectively, corresponding to the formation of the quasi-reversible one-electron reduction Ni(II)/Ni(I) couple. The cyclic voltammogram of Zn(II) complexes did not show any characteristic peak potential in this potential range under similar conditions.

3.6. Thermal study

The thermal stabilities of the complexes were investigated using TG and DTA at a heating rate of 10 °C min^{-1} in N_2 from 35 to 500 °C. The representative TG–DTA curves of CoL_2Cl_2 and $CoL_2(OAc)_2$ complexes are shown in Fig. 4a and b. All the complexes display almost similar decomposition steps. The thermograms showed no weight loss up to 250 °C, indicating stability of the complexes and the absence of water molecule in the complex. In the chloro complexes (Fig. 4a), it is observed that the first thermal degradation that occurs between 250 and 300 °C with an endothermic peak in the range 250–260 °C corresponds to the loss of chloride ions. Above this temperature, a successive decomposition step was observed which can be attributed to the partial decomposition of the Schiff base ligand. This step is accompanied by exothermic peaks. Whereas, in acetato complexes, the first thermal degradation that occurs between 250 and 400 °C corresponds to the loss of acetato groups and partial decomposition of the Schiff base ligand. This step is accompanied by exothermic and endothermic peaks. Based on the above results, the proposed structure of the complexes is given in Fig. 5.

3.7. Powder XRD and SEM

Powder XRD pattern of the Schiff base complexes were recorded over the 2θ = 0–80°. The CoL_2Cl_2 and $CoL_2(OAc)_2$ complexes do not exhibit well defined crystalline peak due to their amorphous

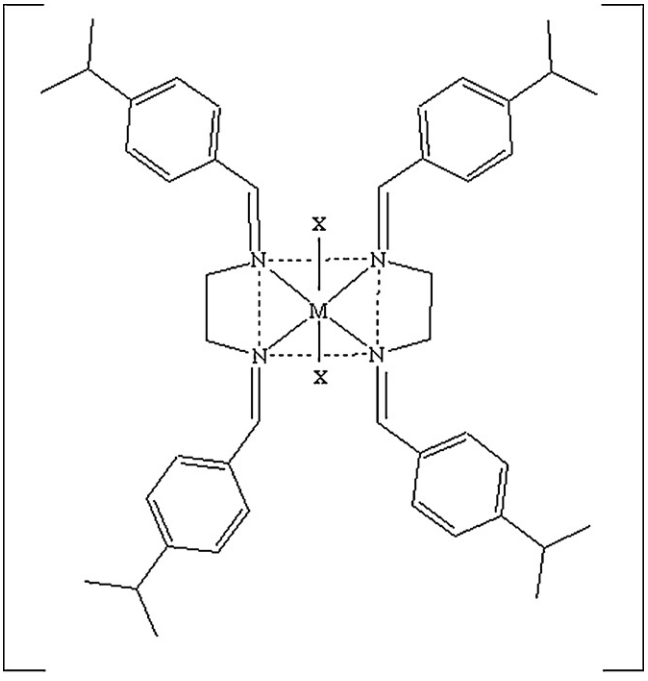

Octahedral geometry

M = Co(II), Ni(II) and Zn(II); X = Cl or OAc

Fig. 5. Proposed structure of the complexes.

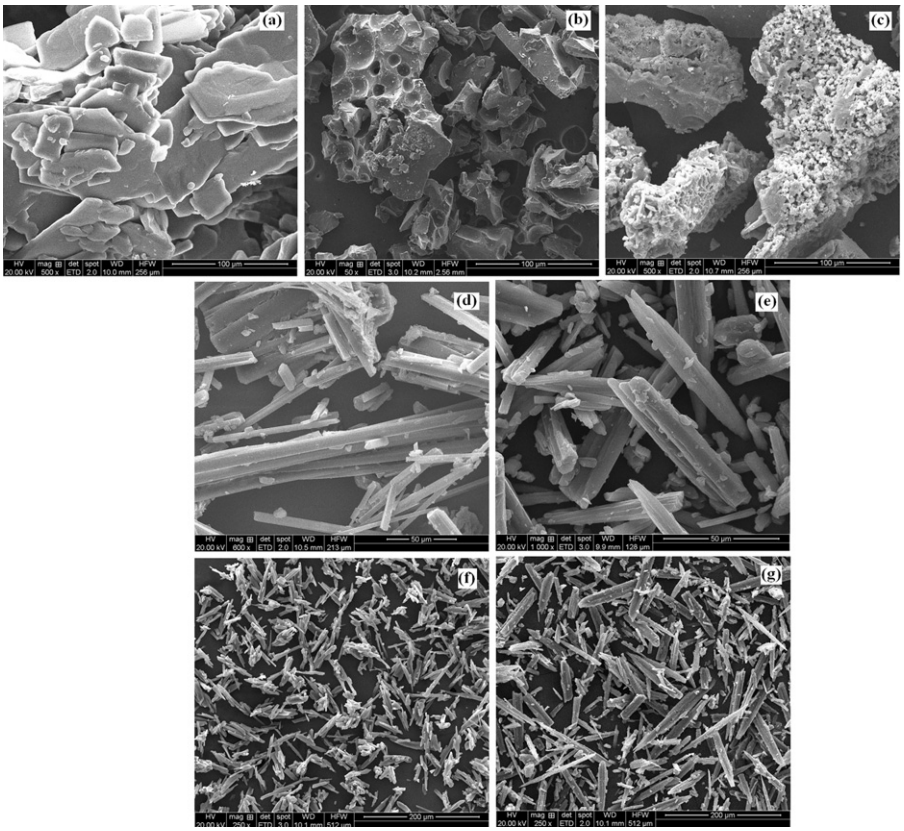

Fig. 6. SEM images of (a) Schiff base ligand (L); (b) $[CoL_2Cl_2]$; (c) $[CoL_2(OAc)_2]$; (d) $[NiL_2Cl_2]$; (e) $[NiL_2(OAc)_2]$; (f) $[ZnL_2Cl_2]$ and (g) $[ZnL_2(OAc)_2]$ complexes.

nature whereas other complexes display sharp crystalline peaks indicating their crystalline nature. The average crystallite sizes of the complexes d_{XRD} were calculated using Scherrer formula [25]. The $[NiL_2Cl_2]$, $[NiL_2(OAc)_2]$, $[ZnL_2Cl_2]$ and $[ZnL_2(OAc)_2]$ complexes have an average crystallite size of 34, 48, 64 and 53 nm, respectively.

The SEM micrographs of the Schiff base ligand (L) and its metal complexes are shown in Fig. 6a–g. The SEM image of Schiff base

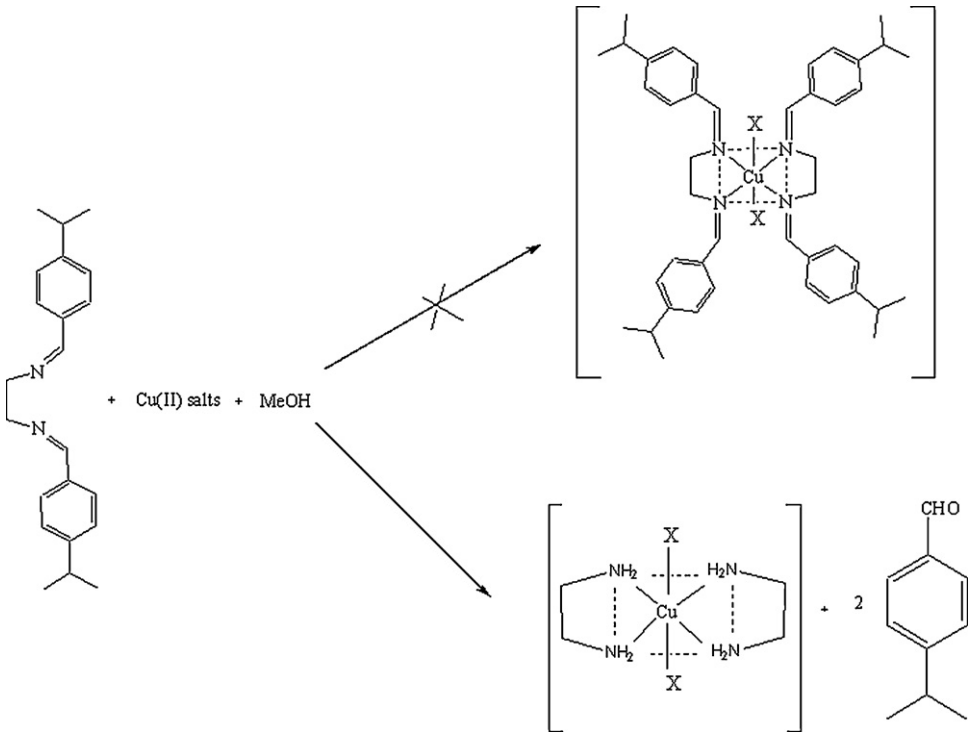

Scheme 1. Complex formation of Cu(II) ion with Schiff base ligand [L].

Table 1
Minimum inhibitory concentration (MIC) results of the synthesized compounds ((g/mL).

Compounds	Bacterial species				Fungal species		
	E. coli	*B. subtilis*	*P. aereuguinosa*	*S. aureus*	*A. niger*	*A. flavus*	*C. albicans*
L	>100	95	>100	95	80	>100	85
$[CoL_2Cl_2]$	25	30	28	35	15	35	15
$[CoL_2(OAc)_2]$	>100	95	95	90	95	>100	>100
$[NiL_2Cl_2]$	15	25	25	85	80	>100	20
$[NiL_2(OAc)_2]$	>100	95	40	90	80	>100	>100
$[ZnL_2Cl_2]$	10	05	20	20	04	04	05
$[ZnL_2(OAc)_2]$	45	25	15	75	75	10	10
Amikascin[a]	15	10	10	05	–	–	–
Ciprofloxacin[a]	15	10	10	10	–	–	–
Ofloxacin[a]	08	10	05	10	–	–	–
Nystatin[a]	–	–	–	–	10	08	08

[a] Standard.

ligand shows (Fig. 6a) irregularly shaped micro flake like surface morphology. The CoL_2Cl_2 complex (Fig. 6b) display agglomerated particles and presence of random distribution of voids in their structure. Whereas $[CoL_2(OAc)_2]$ complex exhibits (Fig. 6c) irregular shaped secondary crystalline object with primary tiny particles. From the SEM image (Fig. 6d and e), it is observed that the crystalline objects are rod-shaped with lateral dimensions in nanometer range but with a considerable length of 50 to few hundred micrometer in the Ni(II) complexes. The SEM image of Zn(II) complexes (Fig. 6f and g) show a gorgeous surface morphology with nano needles and rods, and the presence of particles are randomly distributed.

3.8. Effect of coordination on Cu(II)

Cu(II) reacts with the Schiff base ligand (L) under the normal reaction condition, and undergoes hydrolytic cleavage to form Cu(II)-ethylenediamine complex and the corresponding aldehyde (Scheme 1). The hydrolytic products were isolated and characterized using mass and IR spectroscopic techniques. The cleavage mechanism was not correctly known. However, it is likely that under the conditions of the reaction, an activated nucleophile has been generated at the metal and is responsible for the resultant cleavage reaction [26]. In general, coordination to metal can cause weakening or strengthening of the –C=N– group [27]. Thus, the Cu(II) ion coordinates to the imine nitrogen atom causing the weakening of the –C=N– bond. Consequently, the –C=N– group is highly polarized and nucleophilic attack on the carbon atom of the –C=N– group can occur. This is followed by the presence of water molecule bringing cleavage [27].

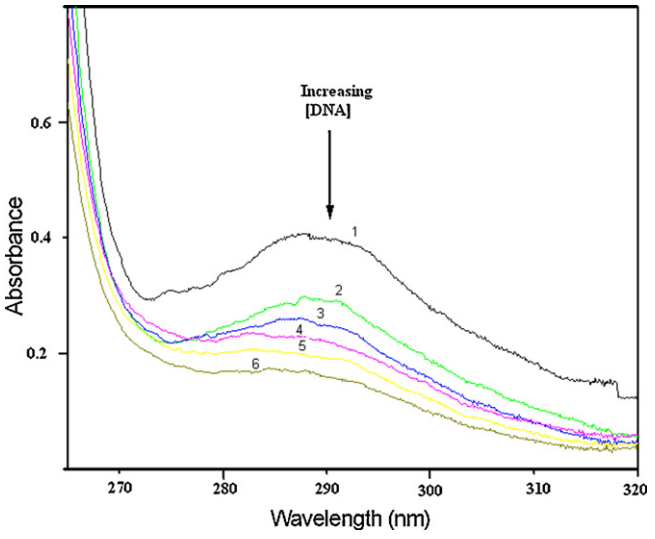

Fig. 7. Absorption spectra of $[ZnL_2Cl_2]$ complex in the presence of increasing amounts of CT DNA. Curve 1: 0 μM DNA + 10 μM $[ZnL_2Cl_2]$; curve 2: 5 μM DNA + 10 μM $[ZnL_2Cl_2]$; curve 3: 10 μM DNA + 10 μM $[ZnL_2Cl_2]$; curve 4: 15 μM DNA + 10 μM $[ZnL_2Cl_2]$; curve 5: 20 μM DNA + 10 μM $[ZnL_2Cl_2]$; curve 6: 25 μM DNA + 10 μM $[ZnL_2Cl_2]$.

4. Biological studies

4.1. Antimicrobial activity

The minimum inhibitory concentration (MIC) values of the compounds are given in Table 1. From the *in vitro* antimicrobial screening results (Table 1), it is observed that the ligand is moderately active against bacteria, *E. coli*, *S. aureus* and fungi, *A. niger*. The complexes have shown higher activity in comparison with the ligand against both bacteria and fungi used. The activity of the ligand has enhanced on complexation, which can be explained on the basis of Overtone's concept and Tweedy's chelation theory [28].

Among the complexes, ZnL_2Cl_2 complex has the highest potential against all the microorganisms, which is even more than the standard drugs used. $[CoL_2(OAc)_2]$ and $[NiL_2(OAc)_2]$ complexes showed lower activity against *E. coli* and *C. albicans* as compared with the free ligand. As seen in Table 1, it can be concluded that the chloro complexes have higher antimicrobial activity than the acetato complexes. This may be due to the presence of labile chloride ions in the complexes [29].

4.2. DNA binding studies

In the UV region, all the complexes exhibit an intense band at 290 nm which is attributed to a π–π^* transition. Upon the addition of CT–DNA to the complexes, a decrease in the molar absorptivity (hypochromism, 23–52%) of the π–π^* absorption band with red shifts is observed, which indicates strong binding of the complexes to DNA. The extent of hypochromism is commonly consistent with the strength of DNA interaction. The observed order of decrease in hypochromism, ZnL_2Cl_2 ($K_b = 5.2 \times 10^5\ M^{-1}$) > NiL_2Cl_2 ($K_b = 1.33 \times 10^4\ M^{-1}$) > CoL_2Cl_2 ($K_b = 6.8 \times 10^3\ M^{-1}$) > $ZnL_2(OAc)_2$ ($K_b = 5.3 \times 10^3\ M^{-1}$) > $NiL_2(OAc)_2$ ($K_b = 5.1 \times 10^3\ M^{-1}$) > $CoL_2(OAc)_2$ ($K_b = 1.25 \times 10^2\ M^{-1}$), reflects the decreasing DNA binding affinities of the complexes in this order. This is consistent with the higher hypochromism and the higher red shift observed for ZnL_2Cl_2. Interestingly, chloro complexes exhibit higher binding affinity than acetato complexes which is also reflected in antimicrobial activity. Complexes bound to DNA through intercalation usually result in hypochromism and red shift due to the intercalative mode involving a strong stacking interaction between the aromatic

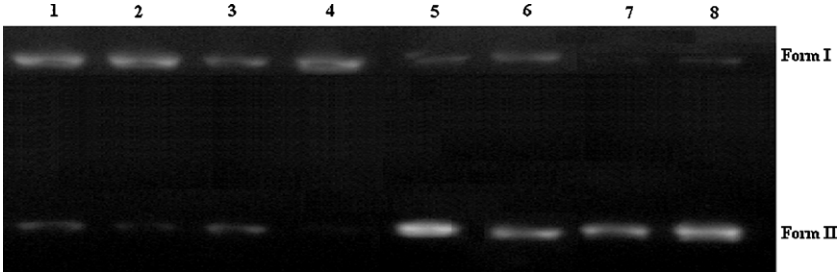

Fig. 8. Gel electrophoresis diagram for the reaction done in the control experiment with an incubation time of 60 min at 30 °C in dark condition: Lane 1: DNA + H_2O_2; lane 2: DNA + Ligand + H_2O_2; lane 3: DNA + $[CoL_2Cl_2]$ + H_2O_2; lane 4: DNA + $[CoL_2(OAc)_2]$ + H_2O_2; lane 5: DNA + $[NiL_2Cl_2]$ + H_2O_2; lane 6: DNA + $[NiL_2(OAc)_2]$ + H_2O_2; lane 7: DNA + $[ZnL_2Cl_2]$ + H_2O_2; lane 8: DNA + $[ZnL_2(OAc)_2]$ + H_2O_2.

chromophore and the base-pairs of DNA [30]. Thus, the above phenomena imply that the present complexes interact with DNA by intercalating mode. The absorption spectrum of the ZnL_2Cl_2 complex in the absence and presence of CT–DNA is shown in Fig. 7

4.3. DNA cleavage studies

Gel electrophoresis experiments using pUC19 DNA were performed with ligand and its metal complexes in the presence of H_2O_2 as an oxidant. At micro molar concentrations for 2 h incubation periods, the ligand (Lane 2) exhibits no significant cleavage activity in the presence of H_2O_2. The nuclease activity is greatly enhanced by the incorporation of metal ion in the respective Schiff base ligand. From Fig. 8, it is evident that the complexes cleave DNA more efficiently in the presence of oxidant, which may be due to the formation of hydroxyl free radicals. These hydroxyl free radicals participate in the oxidation of the deoxyribose moiety, followed by the hydrolytic cleavage of the sugar phosphate backbone. The production of hydroxyl radical due to the reaction between the metal complex and oxidant can be explained as shown below [31].

$$M(II)L + e^- \rightarrow M(I)L$$

$$M(I)L + O_2 \rightarrow M(II)L + O_2{}^-$$

$$2O_2{}^- + 2H+ \rightarrow H_2O_2 + O_2$$

$$M(I)L + H_2O_2 \rightarrow M(II)L + OH^- + OH^\bullet$$

$$O_2{}^- + H_2O_2 \rightarrow O_2 + OH^- + OH^\bullet$$

The cleavage efficiency was measured by determining the ability of the complex to convert the Supercoiled DNA (Form I) to open circular form or nicked form (Form II). As can be seen from Fig. 8, there is a considerable increase in the intensity of bands for open circular form in the case of Ni(II) and Zn(II) complexes compared to that of Co(II) complexes. The different DNA cleavage efficiency of the complexes may be due to the different binding affinity of the complexes to DNA.

5. Conclusion

In Summary, a new Schiff base, *N*,*N*′-bis-(4-isopropylbenzaldimine)-1,2-diaminoethane and its Co(II), Ni(II) and Zn(II) complexes have been synthesized and characterized using various spectroscopic techniques. The results show that the ligand is coordinated to the metal ions in a bidentate manner and the geometrical structures of these complexes are found to be octahedral. The thermograms showed no weight loss up to 250 °C, indicating the absence of water molecule in the complex. The SEM image of Zn(II) complexes show nano needles and rod shaped structure. Coordination with Cu(II) ion with this ligand undergoes hydrolytic cleavage to form ethylenediamine Co(II) complex and the corresponding aldehyde. The complexes can effectively cleave plasmid DNA in the presence of H_2O_2 as an oxidant. Among the complexes, chloroform soluble ZnL_2Cl_2 complex exhibits a good antimicrobial, DNA binding and cleaving properties.

Acknowledgment

One of the authors (D.A) is grateful to National Testing Service-India, CIIL, Mysore for providing the fellowship.

References

[1] V. Mirkhani, R. Kia, A.R. Vartooni, H.K. Fun, Polyhedron 29 (2010) 1600–1606.
[2] M. Xie, X.D. Yang, W. Liu, S. Yan, Z. Meng, J. Inorg. Biochem. 104 (2010) 851–857.
[3] A.G. Montalban, J. Alonso, A.J.P. White, D.J. Williams, Tetrahedron Lett. 51 (2010) 5543–5545.
[4] K. Sundaravel, E. Suresh, M. Palaniandavar, Inorg. Chim. Acta 362 (2009) 199–207.
[5] G.B. Roy, Inorg. Chim. Acta 362 (2009) 1709–1714.
[6] M. Dolaz, V. Mckee, A. Golcu, M. Tumer, Spectrochim. Acta 71A (2009) 1648–1654.
[7] P. Mukherjee, M.G.B. Drew, C.J. Gomez-Garcia, A. Ghosh, Inorg. Chem. 48 (2009) 5848–5860.
[8] B.S. Creaven, M. Devereux, A. Foltyn, S. McClean, G. Rosair, V.R. Thangella, M. Walsh, Polyhedron 29 (2010) 813–822.
[9] S. Kumar, D.N. Dhar, P.N. Saxena, J. Sci. Ind. Res. 68 (2009) 181–187.
[10] K.C. Gupta, A.K. Sutar, Coord. Chem. Rev. 252 (2008) 1420–1450.
[11] P.G. Cozzi, Chem. Soc. Rev. 33 (2004) 410–421.
[12] F. Li, W. Chen, C. Tang, S. Zhang, Talanta 77 (2008) 1–8.
[13] G.H. Clever, M. Shionoya, Coord. Chem. Rev. 254 (2010) 2391–2402.
[14] D.D. Qin, Z.Y. Yang, F.H. Zhang, B. Du, P. Wang, T.R. Li, Inorg. Chem. Commun. 13 (2010) 727–729.
[15] N. Shahabadi, S. Kashanian, F. Darabi, Eur. J. Med. Chem. 45 (2010) 4239–4245.
[16] C.M. Che, F.M. Siu, Curr. Opin. Chem. Biol. 14 (2010) 255–261.
[17] A.I. Vogel, A Textbook of Quantitative Inorganic Analysis Including Elementary Instrumental Analysis, 4th ed., Longman, London, 1978.
[18] A.W. Bauer, W.M.M. Kirby, J.C. Sherris, M. Truck, Am. J. Clin. Pathol. 45 (1966) 493–496.
[19] A.K. Patra, M. Nethaji, A.R. Chakravarty, J. Inorg. Biochem. 101 (2007) 233–244.
[20] W.J. Geary, Coord. Chem. Rev. 7 (1971) 81–122.
[21] G.B. Deacon, R.J. Phillips, Coord. Chem. Rev. 33 (1980) 227–251.
[22] K. Nakamoto, Infrared and Raman Spectra of Inorganic and Coordination Compounds, 3rd ed., John Wiley & Sons, 1978, 91–112.
[23] J.K. Nag, S. Pal, C. Sinha, Trans. Met. Chem. 30 (2005) 523–527.
[24] G.G. Mohamed, C.M. Sharaby, Spectrochim. Acta 66A (2007) 949–958.
[25] C.J. Dhanaraj, M.S. Nair, Eur. Polym. J. 45 (2009) 565–570.
[26] S. Gourbatsis, S.P. Perlepes, I.S. Butler, N. Hadjiliadis, Polyhedron 18 (1999) 2369–2375.
[27] D. Sukanya, M.R. Evans, M. Zeller, K. Natarajan, Polyhedron 26 (2007) 4314–4320.
[28] N.P. Priya, S.V. Arunachalam, N. Sathya, V. Chinnusamy, C. Jayabalakrishnan, Trans. Met. Chem. 34 (2009) 437–442.
[29] A.A. Khandar, B. Shaaban, F. Belaj, A. Bakhtiari, Polyhedron 25 (2006) 1893–1900.
[30] P.K. Sasmal, A.K. Patra, A.R. Chakravarty, J. Inorg. Biochem. 102 (2008) 1463–1472.
[31] B. Macias, M.V. Villa, B. Gomez, J. Borras, G. Alzuet, M.G. Alvarez, A. Castineiras, J. Inorg. Biochem. 101 (2007) 444–451.